Mechanical, electrical and microstructural characterisation of multifunctional structural power composites

Downloaded from: https://research.chalmers.se, 2026-09-09 12:43 UTC

Citation for the original published paper (version of record):
Greenhalgh, E., Ankersen, J., Asp, L. et al (2015). Mechanical, electrical and microstructural characterisation of multifunctional structural power composites. Journal of Composite Materials, 49(15): 1823-1834.
http://dx.doi.org/10.1177/0021998314554

N.B. When citing this work, cite the original published paper.

research.chalmers.se offers the possibility of retrieving research publications produced at Chalmers University of Technology. It covers all kind of research output: articles, dissertations, conference papers, reports etc. since 2004. research.chalmers.se is administrated and maintained by Chalmers Library

(article starts on next page)

Mechanical, electrical and microstructural characterisation of multifunctional structural power composites

E S Greenhalgh[1*], J Ankersen[6], L E Asp[5], A Bismarck[1], Q P V Fontana[2], M Houlle[3], G Kalinka[4], A Kucernak[1], M Mistry[1], S Nguyen[1], H Qian[1], M S P Shaffer[1], N Shirshova[1], J H G Steinke[1] and M Wienrich[4]

[1]Imperial College London, London, SW7 2AZ, UK

[2]Cytec Industrial Materials, Heanor Gate Industrial Estate, Heanor, DE75 7SP, UK

[3]NANOCYL S.A., Rue de l´Essor 4, 5060 Sambreville, Belgium

[4]BAM 5.3, Federal Institute Materials Research & Testing, D-12205 Berlin, Germany

[5]Swerea SICOMP AB, P.O. Box 104, SE-431 22 Mölndal, Sweden

[6]GKN Composites Technology Centre, Bristol, BS16 7FS, UK

* Corresponding author +442075945070 (e.greenhalgh@imperial.ac.uk)

In memoriam of Dr. Joachim H.G. Steinke

Abstract

Multifunctional composites which can fulfil more than one role within a system have attracted considerable interest. This work focusses on structural supercapacitors which simultaneously carry mechanical load whilst storing/delivering electrical energy. Critical mechanical properties (in-plane shear and in-plane compression performance) of two monofunctional and four multifunctional materials were characterised, which gave an insight into the relationships between these properties, the microstructures and

fracture processes. The reinforcements included baseline T300 fabric, which was then either grafted or sized with carbon nanotubes, whilst the baseline matrix was MTM57, which was blended with ionic liquid and lithium salt (two concentrations) to imbue multifunctionality. The resulting composites exhibited a high degree of matrix heterogeneity, with the ionic liquid phase preferentially forming at the fibres, resulting in poor matrix dominated properties. However, fibre dominated properties were not depressed. Thus it was demonstrated that these materials can now offer weight savings over conventional monofunctional systems when under modest loading.
Keywords: Carbon fibres, functional composites, mechanical properties, elastic properties, fractography.

Introduction

Although the development of polymer composites has presented daunting technical challenges, these materials now offer engineers considerable opportunities for efficient structural design. More recently the advent of multifunctional composites, which can fulfil more than one role within a system, has attracted considerable interest and provide designers with exciting opportunities to innovate [1]. Of particular interest are structural power composites [2], which simultaneously carry mechanical load whilst storing/delivering electrical energy. Although the development of these composites is highly challenging, often with conflicting constituent requirements, there has been

considerable success in demonstrating them for automotive applications [3]. This includes small scale demonstration, such as replacing the roof of a radio-controlled car with a structural power material, and production of a larger scale demonstrator: the boot lid of a Volvo S80 in which four stacks of structural power laminates were embedded between composite skins to power the boot light.

The focus of this paper are structural supercapacitors, the basic architecture of a single cell of which is shown in Figure 1a [4]. These entail two carbon fibre woven lamina (electrodes) which sandwich a glass fibre woven lamina (separator), all of which is embedded within a multifunctional matrix (electrolyte). This architecture has been the focus of the research to date, leading to components such as that shown in Figure 1b. Although much of the research effort in structural power has focused on enhancing electrical properties, a critical aspect is ensuring they have competitive mechanical properties. The results reported here are part of a wider study by the STORAGE (Composite Structural Power Storage for Hybrid Vehicles) consortium [5], which led to the fabrication of a set of Devices listed in Table 1. These were chosen to characterise the influence of different reinforcements and matrix developments on the electrical and mechanical performance of the resulting multifunctional composites. Although the reinforcement constituents were not degraded by the modifications used to enhance electrical performance, imbuing ionic conductivity inherently softens the matrix. The aim of the work described here was to characterise critical mechanical properties of

these multifunctional materials, and to understand the relationships between these properties, the microstructures and fracture processes, as well as the electrical properties. Adoption of structural power materials would be a considerable step change in design philosophy, and the ambition is that these materials will reach a level of performance that can offer real savings. To this end O'Brien [6] has presented an approach to assess as to whether such materials would offer a weight saving: this paper culminates in such an analysis of the materials reported here.

Experimental

Materials and fabrication

As detailed in Table 1, four structural supercapacitor configurations and two structural baselines were investigated in which the reinforcement and matrix constituents were changed. T300 3k carbon fibre fabrics (twill weave) and glass fibre fabrics (plain weave) were used as the electrode and separator reinforcements, respectively. Although the baseline fabric was as-received, two carbon nanotube (CNT) reinforced configurations, as developed by Nanocyl, were also investigated; *T300 CNT* had CNTs grafted onto the fibre surfaces whilst *T300 AquaCyl* had a CNT sizing. Details of the synthesis of these reinforcement systems are given in [7]. Regarding the matrix, the baseline was MTM57, which is a prepreg fully formulated epoxy system prepared by Cytec Industrial Materials. To imbue this with ionic conductivity, this epoxy was blended with an equal weight fraction of ionic liquid (1-ethyl-3-methylimidazolium

bis(trifluoromethylsulfonyl) imide) and either of two concentrations of lithium bis(trifluoromethane)sulfonimide (LiTFSI); *conc1* (2.3 mol/l) and *conc2* (4.6 mol/l). These different constituents where brought together to produce the four different multifunctional Devices as shown in Table 1. These were compared against Device A: a monofunctional structural baseline (T300/Cytec MTM57). In addition, to characterise the effect of CNT reinforcement on the mechanical properties, Device F was fabricated using CNT grafted fibres with the structural matrix (MTM57). Details of the matrix synthesis and processing are given in [8], but the laminates were made via a prepregging route [2], producing Devices 180mm x 180mm in size (Figure 2). Prior to prepregging, a 10mm wide adhesive copper strip was attached to each carbon layer, and these were then laid up such for each pair of electrodes the copper strip was on opposing edges, as seen in Figure 2. Directly following fabrication the laminates were sealed in polymer film to avoid exposure to ambient moisture, and electrical testing was undertaken in a glovebox in a dry atmosphere (below 50 ppm moisture). After electrical testing, these laminates were then cut into mechanical test specimens (see next Section) using a dry diamond saw, but again kept dry in a vacuum oven prior to testing.

Characterisation

The electrical characterisation of the laminates was conducted on the $[\pm CF/\pm GF]_S$ laminates prior to cutting (Figure 2). Voltage chronoamperometry was used, in which an applied voltage ($U_{applied}$) of 0V to 1V for 4000s was applied followed by another step in

potential from 1V to 0V for a further 4000s. This was then used to deduce the electrical properties by fitting the electrical behaviour to a Randles Circuit (Figure 3) as described in Reference [4]. This gave the following parameters: a capacitance of C_{SP}, a parallel resistance, R_P, and an equivalent series resistance (ESR), R_S. A high performance supercapacitor requires large values of C_{SP} and R_P and low values of R_S. Consequently, the energy (Γ) and power (P) densities were determined as follows:

$$\Gamma = \frac{1}{2} C_{SP} U_{\text{int}}^2 \qquad \text{(Equation 1)}$$

$$P = \frac{U_{\text{int}}^2}{4R_S} \qquad \text{(Equation 2)}$$

where $U_{Int} = \frac{R_p}{\left(R_p + R_S\right)} U_{applied}$.

Since imbuing the matrix with electrical characteristics had been seen to reduce its mechanical properties [4], characterisation focused on matrix and fibre/matrix dominated properties of the resulting composites. Firstly, in-plane shear modulus and strength of the supercapacitors was characterised using the ±45° tension test [9] with a $[\pm CF/\pm GF]_S$ laminate. This test method provided direct comparison with the results of previous studies [2], and illustrated how the structural supercapacitors would behave under realistic loading conditions. However, a particular concern was the negative influence of the multifunctional matrix on the load-bearing layers, and therefore in-plane (0°/90°) compression properties were characterised using $[CF_4]_S$ laminates

containing just the electrode material [10]. It was recognised that compression loading of the hybrid glass/carbon laminates would have probably resulted in delamination before microbuckling of the load-bearing layers could have developed, and therefore would have limited any understanding gleaned of this critical property. However, using compression data for multifunctional design would require the hybrid composite to be characterised. At least five specimens were tested per condition. In addition, the volume fraction of the fibres was measured using Procedure B from the ASTM standard D3171 [9].

Following testing, the microstructure and the fracture morphology of the composites were characterised using a Hitachi S3700N-II scanning electron microscope. Prior to examination, these specimens were sputter coated with gold. It should be noted that the ionic liquid had not been removed, which reduced the resolution of the subsequent electron micrographs. However, it was felt that any attempt to remove the ionic liquid may have led to artefacts being introduced onto the fracture surfaces. Finally, polished sections were also taken of pristine $[CF_4]_S$ laminates to study the microstructure: these were examined using an optical (Zeiss Axio M2m) microscope.

Results and discussion

Microstructures

Typical polished sections of the pristine $[CF_4]_S$ laminates are shown in Figure 4. The structural baseline (Device A) had a microstructure typical of that of a good quality

woven CFRP laminate, with a uniform interply spacing, good fibre/matrix interface and negligible voidage or fibre misalignment (Figure 4a). The baseline multifunctional configuration (Device B) exhibited a high degree of heterogeneity in the matrix microstructure (Figure 4b). Within and close to the fibre tows there was a dominance of ionic liquid in the matrix whilst away from the tows (i.e. in the interstitial sites between the tows), large 'islands' of structural epoxy were apparent. These consisted of sites typically of the order of 500 microns in size, containing a skin/core structure (i.e. the outer surface was smooth whilst the interior contained small isolated pores). Finally, some evidence of voidage at the interlaminar interfaces was apparent.

As shown in Figure 4c, CNT grafting on the fibres in the multifunctional composite (Device C) led to superior consolidation, matrix stiffness and less voidage compared to that of Device B. The matrix was again heterogeneous, with the epoxy phase dominating at the interstitial sites. Doubling the concentration of the lithium salt in this configuration (Device D) led to a subtle change in the morphology (Figure 4d), with larger pores in the epoxy dominated regions. Changing from grafted to CNT sizing (Device E) led to reduced voidage and hence a superior microstructure (Figure 4e). Finally, as shown in Figure 4f, structural epoxy with CNT grafted carbon fibres (Device F) had a microstructure almost identical to that of the structural baseline (Device A).

Electrical results

The electrical results are tabulated in Table 2. The capacitances of the devices ranged from 4.80mF g^{-1} (Device E) to 10.04mF g^{-1} (Device D), which was very low as compared to that of a conventional supercapacitor (2800 mF g^{-1}) [12]. This poor specific capacitance was associated with the low surface area of the reinforcements, suggesting approaches such as carbon aerogel coating of the fibres, as reported in [7] and [13], should be pursued. Although the parallel resistance of all the Devices was generally high, the ESR was also high, ranging from 383 kΩ cm^2 (Device D) to 1751 kΩ cm^2 (Device C): in comparison a conventional supercapacitor has an ESR of the order of milliohms [12]. The poor ESR of the multifunctional devices was perhaps associated with the poor ionic conductivity of the matrix, as shown in [8] and the relatively large spacing between the electrodes as compared to that in conventional supercapacitors.

In-plane shear results

The in-plane shear strength and moduli are tabulated in Table 2. The structural baseline (Device A) had a strength and stiffness typical of a woven CFRP laminate with a structural epoxy [14]. Similarly, the structural epoxy with CNT grafted fibres (Device F) had a reasonable in-plane shear performance, although inferior to that of the structural baseline. Both these Devices had failed via translaminar fracture of the fibres following necking (and some scissoring of the plies), as is typical for this test condition [15]. However, the introduction of the ionic liquid (Device B) led to a greatly reduced

in-plane shear stiffness and strength; of the order of 10% of the performance of the structural baseline. The presence of the CNTs (particularly for Devices C and E) recovered some of this performance, with these materials having about 25% and 22% of the shear stiffness and strength respectively of the structural baseline.

In-plane Compression results

The in-plane compression strength and moduli are tabulated in Table 2 with typical fracture modes presented in Figure 5. Although the laminates were fabricated using a prepreg route, because of the highly unusual nature of the matrix, the prepreg manufacture aimed for a fibre volume fraction of between 50 and 55%. However, for the CNT sized and grafted laminates (Devices C to F) the pretreatment of the dry fabrics tended to make them more 'fluffy'. In some cases this led to poorer packing of the tows, and therefore lower fibre volume fractions, which could potentially be a critical issue for future adoption of CNT reinforced materials. It was noted that the structural baseline (Device A) also had a low volume fraction, and it was not clear as to why this was. Because of this variation in the fibre volume fraction between the Devices, the compressive moduli were normalised to a fibre volume fraction of 55% using Equation 3, which assumes negligible contribution from the matrix, to allow direct comparison between the results, where $\overline{E}$ was the volume fraction normalised modulus, E was the measured modulus and v_f was the fibre volume fraction.

$$\overline{E} = E\frac{0.55}{v_f} \qquad \text{(Equation 3)}$$

The structural baseline (Device A) had a strength and stiffness typical of a woven CFRP laminate with a structural epoxy [16]. Furthermore, this exhibited (Figure 5a) a fairly localised compression failure, which was consistent with there having been limited delamination formation during failure [15]. Similarly, the structural epoxy with CNT grafted fibres (Device F) had a slightly inferior compressive strength (82%) to that of the structural baseline. As can be seen in Figure 5, this Device exhibited an increased propensity to delamination compared to that of the structural baseline.

As can be seen in Table 2, an encouraging observation was that the normalised moduli of the composites were relatively insensitive to the matrix formulation. This would suggest that under relatively modest loading the softer matrix would not disadvantage the mechanical performance of the material, which bodes well for using these materials in structural applications.

Considering the influence of the multifunctional matrix on the in-plane compression strength (Table 2), as had been seen with the in-plane shear results, there was a large drop in performance. The multifunctional baseline (Device B) exhibited over a 50% reduction in strength as compared to the structural baseline (Device A). This was attributed to the heterogeneity of the matrix, which was dominated by the ionic liquid phase adjacent to the fibres (Figure 4b). This would have led to reduced fibre support,

and promotion of fibre/matrix debonding. Device B (Figure 5) had a localised translaminar failure, which was consistent with there having been negligible delamination during failure [15].

It was evident that introduction of grafted CNTs to this multifunctional matrix (Device C) had not recovered the in-plane compressive performance. Furthermore, increasing the LiTFSI concentration (Device D) or using CNT sized fibres (Device E) led to even further reductions in in-plane compressive strength; 25% of that of the structural baseline (Device A). It was apparent that these three Devices had exhibited significant delamination prior to compressive failure, since the failure mode was ‘green stick’ [15].

Fractographic observations

Following mechanical testing of the ±45° in-plane shear specimens, all but the structural baseline (Device A) were found to have delaminated at the glass fibre/carbon fibre ply interface. These surfaces were subsequently exposed to allow characterisation of the matrix morphology, and relate it to that observed in the bulk matrix studies [8]. Figure 6 shows typical delamination morphology for all the multifunctional devices. There was a high degree of heterogeneity, and in particular, the ionic liquid constituent was dominant close to the fibres, whilst in the interstitial sites (i.e. tow cross-over points), the structural epoxy had dominated.

The multifunctional baseline (Device B) presented voidage at the ply interface, but the matrix exhibited a porous structure, as illustrated in Figure 6a. It should be noted that

these pores are not voids, but would have contained ionic liquid. The pores varied in size, from 1 to 10 microns, and did not appear to be interconnected.

Further detail of this microstructure, and the morphology close to the fibre/matrix interface, is shown in Figure 7. The detail of the bonding between the fibres and matrix can be seen, which illustrates that adhesion was fairly heterogeneous with localised regions with no mechanical bond (but good ionic conductivity). However, in some isolated regions, sheathing of the fibres by the structural phase of the matrix was identified (Figure 8). Here it was apparent that there was no direct contact between the fibres and the ionic liquid (i.e. pores). Such sites would insulate the active electrode (fibres) from the electrolyte, leading to poor electrical properties. However, as noted earlier, in general the ionic liquid dominated the matrix directly adjacent to the fibres.

As can be seen in Figure 6, the addition of CNTs to the fibres (Devices C, D and E) led to enhanced matrix wetting of the tows during fabrication, since the degree of voidage was less than that of the baseline multifunctional (Device B). Firstly consider the carbon fibres with grafted CNTs, with a lithium salt concentration of 2.3 mol/l (Device C). The morphology of the matrix was akin to that of Device B, with a porous structure throughout the matrix. However, in some regions (Figure 9), beads of structural matrix were apparent. These were sites at which there had been a higher concentration of the ionic liquid, leading to the structural epoxy having formed isolated beads of material. Clearly such sites would have had poor structural performance, but superior ionic

conductivity. Finally, the bonding between the carbon fibres and the matrix exhibited pores adjacent to the fibres which would have facilitated good ionic access.

Next consider the influence of increasing the concentration of the lithium salt to 4.6 mol/l on the composite morphology. The consolidation of the composite was good, but the matrix morphology differed from that of the lower lithium salt concentration, as can be seen in Figure 6c, and in detail in Figure 10. In this instance, the matrix was much more heterogeneous, with large 'islands' (up to 200 microns in size) containing agglomerations of the bead-like features. These islands are within a 'sea' of structural polymer with very fine pores (the order of 1 micron in size). Similarly, the wetting of the carbon fibres by the matrix was more heterogeneous, with large regions dominated by ionic liquid, whilst other areas in which structural epoxy/fibre bonding was present.

Finally, the influence of CNT sizing rather than CNT grafting was characterised by examination of Device E (Figure 6d). This exhibited relatively good bonding between the glass and carbon fibre layers although there were some regions of large voids. However, as shown in Figure 11, there were subtle differences in the microstructure. In particular, in some regions close to the fibres the structural matrix had formed an almost skeletal microstructure, with large pores next to the fibres. Away from these sites the structural phase was dominant, with only small, localised pores present.

Multifunctional analysis

The aim of this work was to characterise critical mechanical properties of structural supercapacitors, and to understand the relationships between these properties and the microstructure and fracture processes. However, critical to evaluating the mechanical performance is the balance with the electrical properties. Due to the dual mechanical and electrical requirements, this balance consequently leads to conflicting microstructures: rigid and solid microstructures for mechanical performance, whilst porous and non-tortuous microstructures for ionic conductivity.

Such a conflicting balance could be to the detriment to the uptake of these materials, since they may not offer an overall weight saving over existing systems. (i.e. a structural component plus an energy storage device). O'Brien [6] has demonstrated that a multifunctional material can offer a weight saving if the multifunctional efficiency, η_{mf}, exceeds unity:

$$\eta_{mf} \equiv \eta_e + \eta_s > 1 \qquad \text{where } \eta_e = \frac{\bar{\Gamma}_{mf}}{\bar{\Gamma}} \ \& \ \eta_s = \frac{\bar{E}_{mf}}{\bar{E}}$$

where η_e and η_s are the electrical and mechanical efficiencies of the multifunctional material, Γ and Γ_{mf} are the specific energy densities of the conventional device and multifunctional system respectively, and E and E_{mf} are the specific moduli of the conventional and multifunctional materials respectively. It should be noted that the selection of the pertinent electrical and mechanical parameters for analysis of the

material will depend upon the application. To analyse the results reported here, STORAGE Device A was deemed the structural material whilst the monofunctional electrical device considered was a Maxwell BCAP0010 10F supercapacitor [12]. The energy densities for Devices B to E are presented in Table 2.

Figure 12 shows the multifunctional efficiencies (η_{mf}) for the four multifunctional materials (Devices B, C, D and E) for fibre dominated (normalised Young's modulus) and matrix dominated (Shear Modulus) properties. Firstly, consider the normalised Young's modulus (fibre dominated behaviour), which is probably the most important parameter for engineering design. In this instance, because the reinforcement has not been degraded by the modification used to imbue the electrical characteristics [7], all these materials are approaching offering a weight saving over conventional (monofunctional) systems: in fact Device C just exceeds unity. This is encouraging since, despite the electrical properties of these Devices being poor, it implies these materials can very soon be utilised in moderately loaded or perhaps even purely tension loaded applications. However, it should be noted that the normalisation assumes that these laminates would behave in the same manner of conventional composites such that modulus was directly proportional to fibre volume fractions.

When considering matrix dominated behaviour (shear modulus), the soft matrix is considerably detrimental to mechanical performance, and hence multifunctional efficiencies, with η_{mf} of at best 0.30 (Device C). This implies more research is required

before these materials will offer weight savings in matrix dominated loading conditions, such as compression, shear or bending.

Concluding remarks

The research reported here provides an insight into the influence of the different constituents (enhanced reinforcements and multifunctional matrices) on the mechanical and electrical properties, microstructures and fracture processes of structural supercapacitors. Both the reinforcement type and the matrix formulation had a strong influence on the resulting microstructure, with the latter presenting significant heterogeneity. This heterogeneity was perhaps associated with the presence of the fibres disrupting the equilibrium between the different phases during cure: the observations suggest that ionic liquid dominated phases preferentially formed near the fibres, leading to depletion of ionic liquid remote from the fibres, and therefore structural dominated phases at the interstitial sites. To achieve good control over the matrix microstructure, as had been achieved in the bulk [8], this issue will need to be addressed.

The work reported has illustrated how the resulting microstructure then influenced the mechanical properties. In general, the porous multifunctional matrix and the dominance of ionic liquid at the fibre/matrix interfaces, depressed matrix dominated properties. This would suggest further optimisation of the matrix, such as tailoring the wetting of the fibres by the different matrix phases, is necessary to achieve a good balance between

electrical and mechanical properties. However, the observations in this paper do provide an insight to direct future refinement and optimisation of these materials.

It should be noted that the Devices were kept dry during both electrical and mechanical testing. In practice, such multifunctional materials would be hybridised with conventional composites to both isolate them from ambient moisture and to electrically isolate them.

The structural supercapacitors presented here can now provide a weight saving compared to conventional (monofunctional) systems when used in modest (fibre dominated) loading conditions, but still need further development to address matrix dominated strengths, such as under in-plane compression or in-plane shear stress. Overall, the findings of this multifunctional analysis provides a route to exploitation of structural supercapacitors, since they could find use in the near term for lightly loaded applications, such as tertiary or secondary structures.

Acknowledgments.

The work was funded by EU FP7 programme StorAGE (Proposal 234236). The authors would like to thank Mr Richard Shelton from Cytec Industrial Materials for help with composites manufacturing.

References

[1] R. F. Gibson. “A review of recent research on mechanics of multifunctional composite materials and structures”. *Composite Structures*. Vol. 92, No. 12, pp 2793-2810, (2010).

[2] L. E. Asp, E.S. Greenhalgh, “Structural Power Composites”, *Composites Science and Technology*, Vol. 101, pp41–61 (2014).

[3] M. Mistry, A. Kucernak, S. Nguyen, J. Ankersen, E.S. Greenhalgh, “Addressing Engineering Issues for a Composite Structural Power Demonstrator”, ICCM19, Montreal, Canada, (2013).

[4] N. Shirshova, H. Qian, M. S. P. Shaffer, J. H. G. Steinke, E. S. Greenhalgh, P. T. Curtis, A. Kucernak and A. Bismarck. “Structural composite supercapacitors”. *Composites: Part A*. Vol. 46, pp 96-107, (2013).

[5] Composite Structural Power Storage for Hybrid Vehicles Structural (StorAGE), FP7 Proposal 234236, (2010).

[6] O'Brien D J, Baechle D M, Wetzel E D., “Design and performance of multifunctional structural composite capacitors”, *Journal of Composite Materials* 45(26): 2797-2809, (2011).

[7] Qian, H., Diao, H., Houllé, M., Amadou, J., Shirshova, N., Greenhalgh, E.S., Shaffer, M.S.P, Bismarck, A., *Carbon Fibre Modifications for Composite Structural*

Power Devices, ECCM 15 - 15th European Conference on Composite Materials, Venice, Italy, (2012).

[8] Shirshova, N., Bismarck, A., Carreyette, S., Fontana, Q.P.V., Greenhalgh, E.S., Jacobsson, P., Johansson, P., Marczewski, M.J., Scheers, J., Kalinka, G., Kucernak, A., Shaffer, M.S.P., Steinke, J.H.G., Wienrich, M., Structural Electrolytes for Supercapacitors Based on Ionic Liquid Doped Epoxy Resins, *Journal of Materials Chemistry*, 1, 5300-15309, (*2013*) (2013).

[9] ASTM International. Standard Test Method for Tensile Properties of Polymer Matrix Composite Materials, ASTM D3039-08, (2008).

[10] ISO. Fibre-reinforced plastic composites — Determination of compressive properties in the in-plane direction, DIN EN ISO 14126, (1999).

[11] ASTM International. "Standard Test Methods for Constituent Content of Composite Materials; Procedure B", ASTM Standard D3171-99 (1999).

[12] Maxwell BCAP0010 datasheet www.maxwell.com/products/ultracapacitors/docs/datasheet_hc_series_1013793.pdf, (Accessed 27th January 2014).

[13] Qian, H., Kucernak A.R.J., Greenhalgh, E.S., Bismarck, A., Shaffer, M.S.P., Multifunctional Structural Supercapacitor Composites Based on Carbon Aerogel Modified High Performance Carbon Fibre Fabric, *ACS Applied Materials & Interfaces* 5(13), (2013), 6113-6122.

[14] K. Gliesche, T. Hübner, H. Orawetz,"Investigations of in-plane shear properties of ±45°-carbon/epoxy composites using tensile testing and optical deformation analysis", *Composites Science and Technology*, 65 (2), pp 163-171, (2005).

[15] E.S. Greenhalgh, "Failure Analysis and Fractography of Polymer Composites", Woodhead Publishing, (2009).

[16] S. T. Pinho, R. Gutkin, S. Pimenta, N. V. De Carvalho, and P. Robinson, "On longitudinal compressive failure of carbon-fibre-reinforced polymer: from unidirectional to woven, and from virgin to recycled", *Phil. Trans. R. Soc. A*, 370 1965, pp1871-1895, (2012).

Tables

Table 1 Device configurations (multifunctional composites are shown in light grey).

#	Type	Electrode	Matrix*†
A	Structural Baseline	T300 fabric	MTM57
B	Multifunctional Baseline	T300 fabric	MTM57:IL+LiFSI[2.3mol/l]
C	CNT Grafted Multifunctional (conc1)	T300 CNT	MTM57:IL+LiFSI [2.3mol/l]
D	CNT Grafted Multifunctional (conc2)	T300 CNT	MTM57:IL+ LiFSI [4.6mol/l]
E	CNT Sized Multifunctional (conc1)	T300 AquaCyl	MTM57:IL+ LiFSI [2.3mol/l]
F	CNT Grafted Structural	T300 CNT	MTM57

*IL (1-ethyl-3-methylimidazolium bis(trifluoromethylsulfonyl) imide);
† LiTFSI (lithium bis(trifluoromethane)sulfonimide)

Table 2 Mechanical and electrical performance for the six different devices.

Device	**Shear Modulus G_{12} / GPa**	**Shear Strength τ_{12} / MPa**	**v_f**	**Compression Strength X_C / MPa**	**Compression Modulus E_c / GPa**	**Normalised‡ Compression Modulus E_c / GPa**	**Capacitance C_{SP} / mF g^{-1}**	**ESR R_S / kΩ cm^2**	**Parallel Resistance R_P / kΩ cm^2**
Device A Structural Baseline	3.52±0.16	106.04±3.66	45%	619.1±36.8	53.6±3.83	65.0±4.65	-	-	-
Device B Multifunctional Baseline	0.41±0.21	9.21±1.18	51%	292.3±33.4	58.5±4.71	63.4±5.10	6.98	852	7832
Device C CNT Grafted Multifunctional (conc1)	1.04±0.08	25.48±3.44	44%	294.9±9.5	52.0±4.83	65.0±6.05	5.00	1751	8187
Device D CNT Grafted Multifunctional (conc2)	0.45±0.05	14.09±0.48	42%	153.2±14.4	46.9±5.61	61.2±7.33	10.04	383	1555
Device E CNT Sized Multifunctional (conc1)	0.85±0.18	22.48±3.51	49%	170.2±7.2	47.5±4.96	53.2±5.55	4.80	1063	677
Device F CNT Grafted Structural	3.11±0.13	80.13±1.56	59%	506.6±37.1	60.6±5.23	56.9±4.91	-	-	-

*****Assuming 2.7V applied: ‡normalised to v_f=55%

Figures

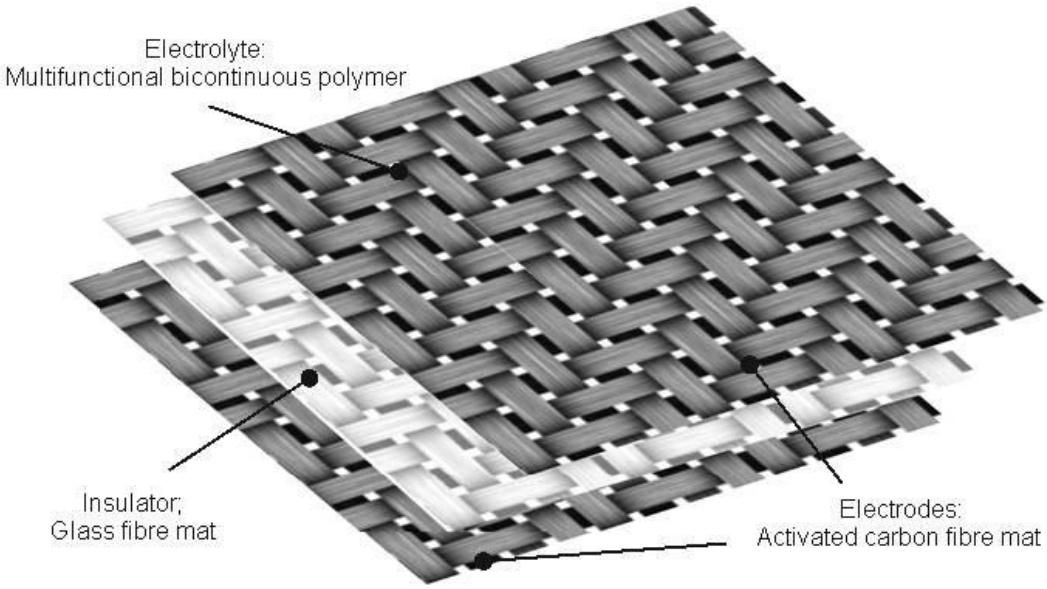

(a)

(b)

Figure 1 (a) Architecture of the structural supercapacitors and (b) example of a working device.

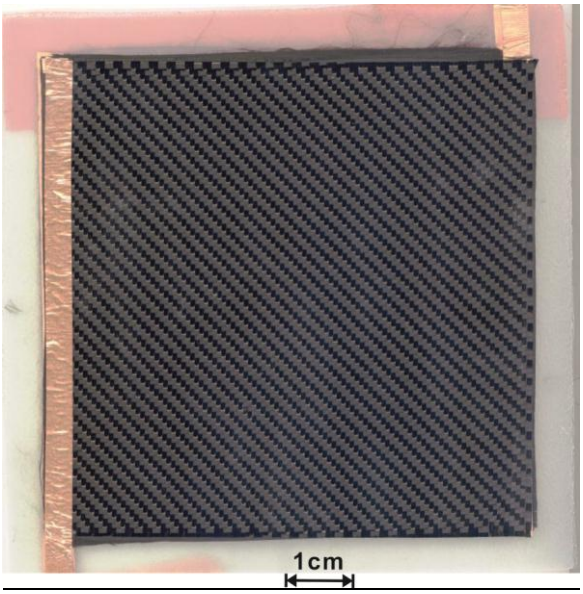

Figure 2 Example of multifunctional laminate with copper strips attached.

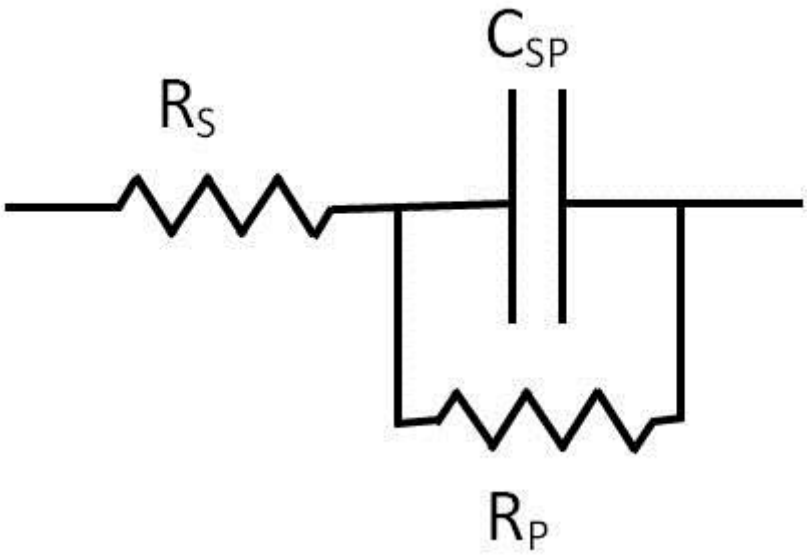

Figure 3 Equivalent (Randles) circuit for supercapacitor system.

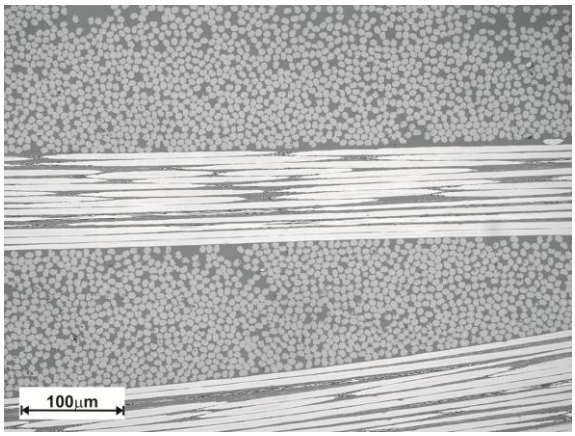

(a) Device A
Structural Baseline

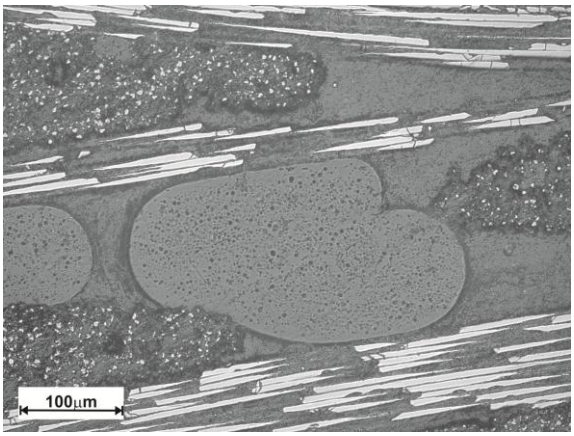

(b) Device B
Multifunctional Baseline

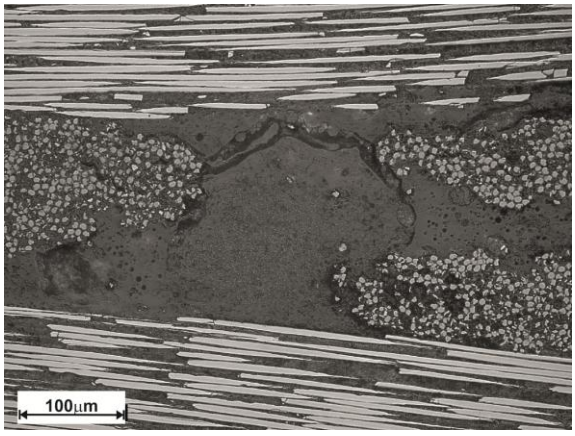

(c) Device C
CNT Grafted Multifunctional (conc1)

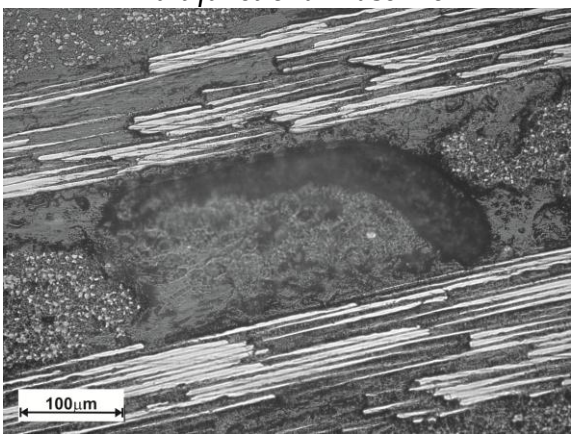

(d) Device D
CNT Grafted Multifunctional (conc2)

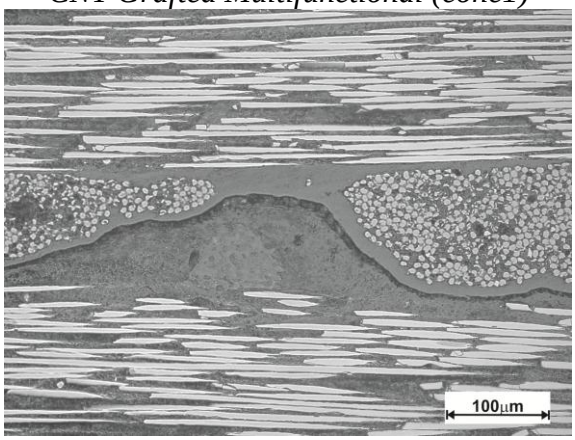

(e) Device E
CNT Sized Multifunctional (conc1)

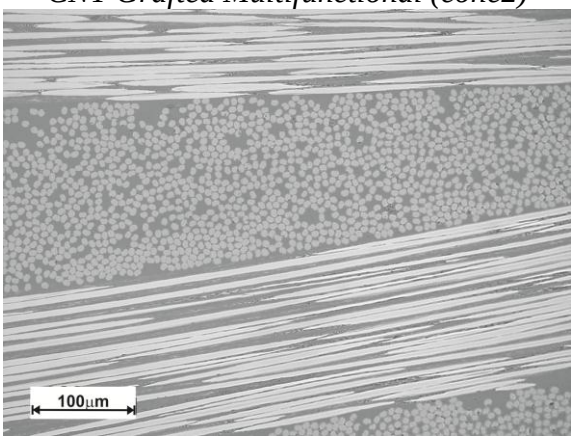

(f) Device F
CNT Grafted Structural

Figure 4 Polished Sections of the Six Different Devices.

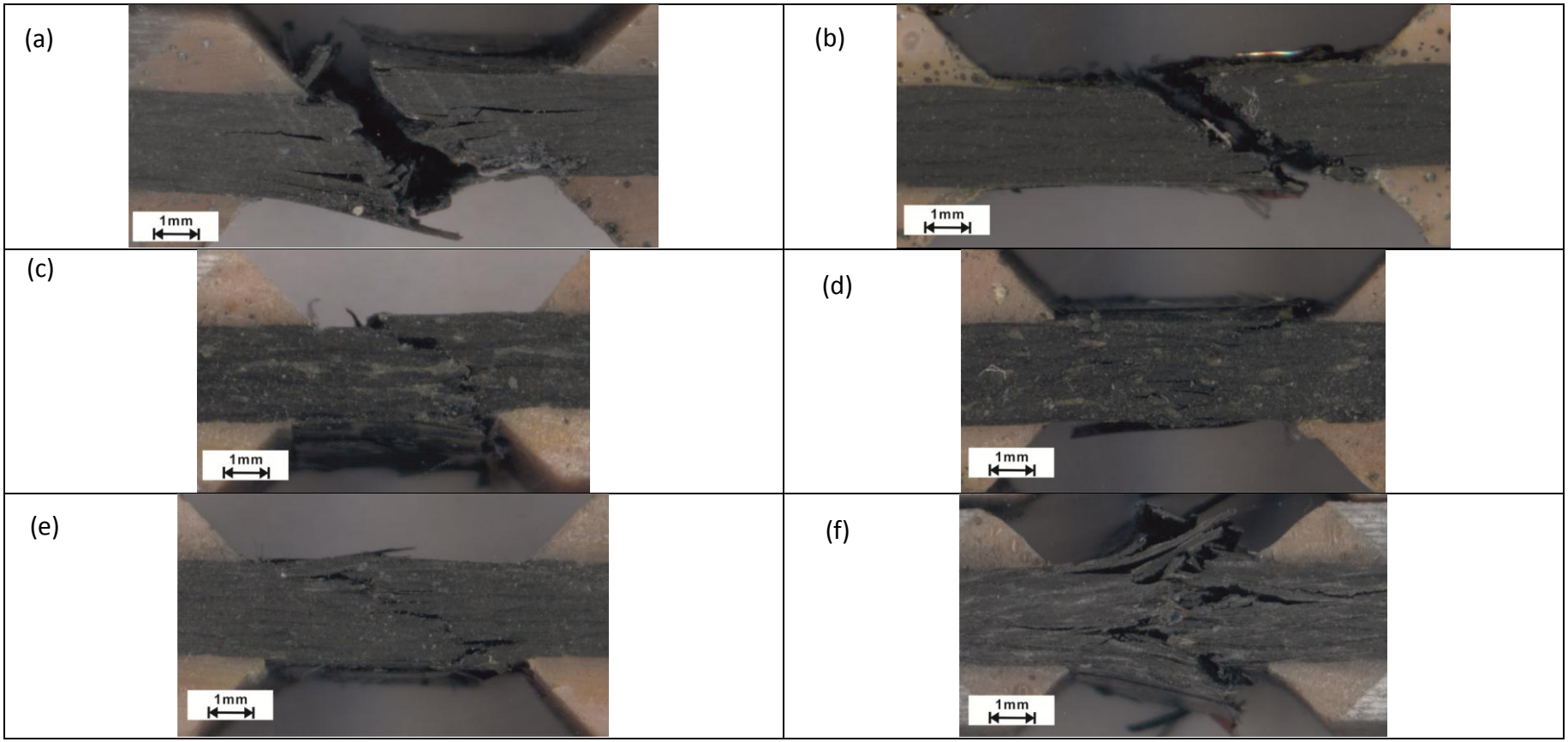

Figure 5 In-plane compressive failure modes for Device A (*structural baseline*), Device B (*multifunctional baseline*), Device C (*CNT Grafted Multifunctional conc1*), Device D (*CNT Grafted Multifunctional conc2*), Device E (*CNT Sized Multifunctional conc1*) and Device F (*CNT Grafted Structural*).

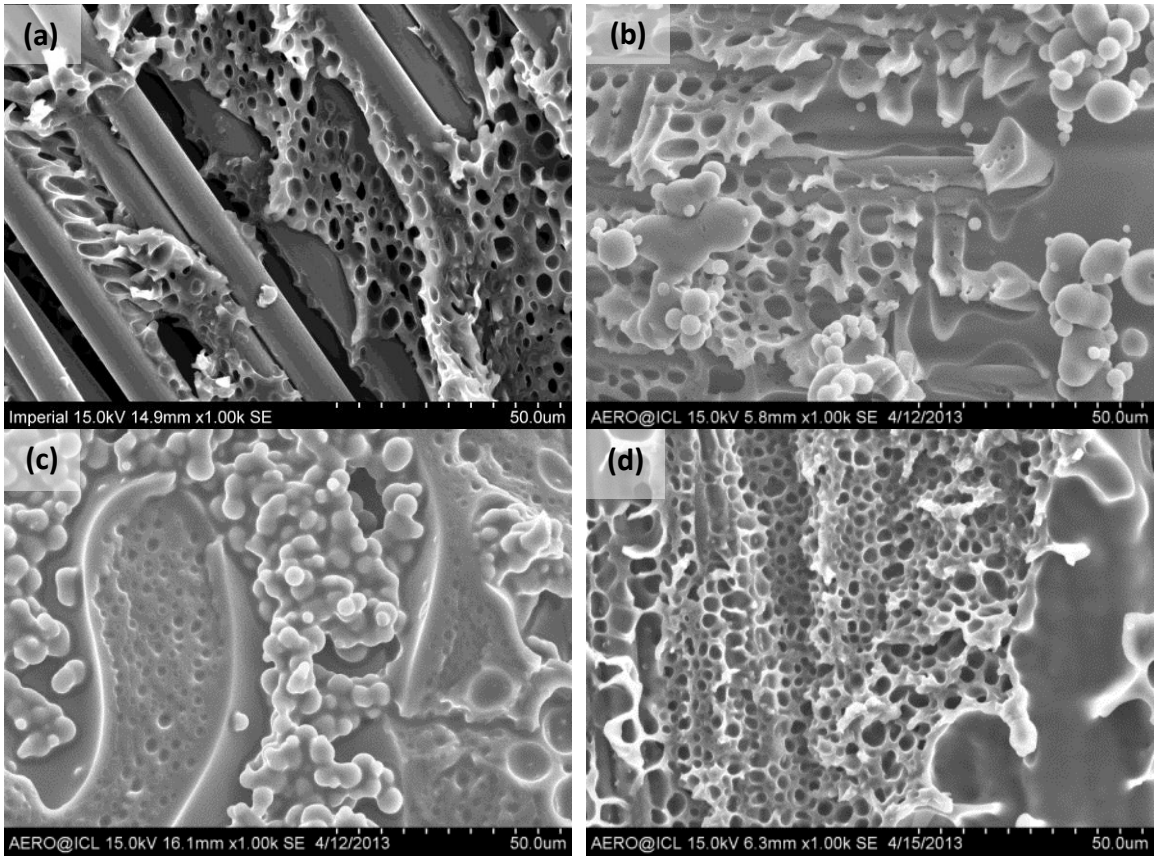

Figure 6 Morphology of the glass-fibre delamination surface in (a) Device B (*Baseline multifunctional*), (b) Device C (*CNT Grafted Multifunctional conc1*), (c) Device D (*CNT Grafted Multifunctional conc2*) and (d) Device E (*CNT Sized Multifunctional conc1*). N.B. Number below the scale bar indicates its full extent.

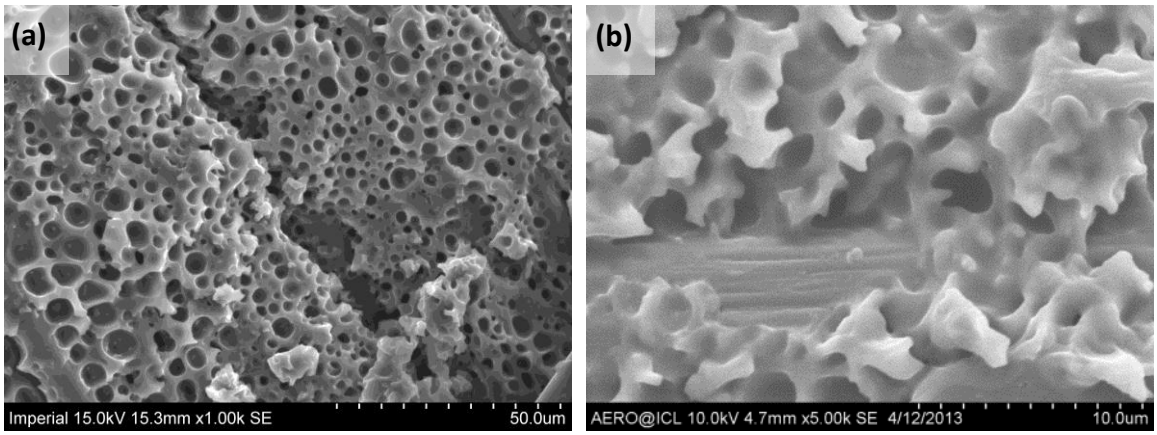

Figure 7 Detail of the matrix morphology in Device B (*Baseline Multifunctional*). N.B. Number below the scale bar indicates its full extent.

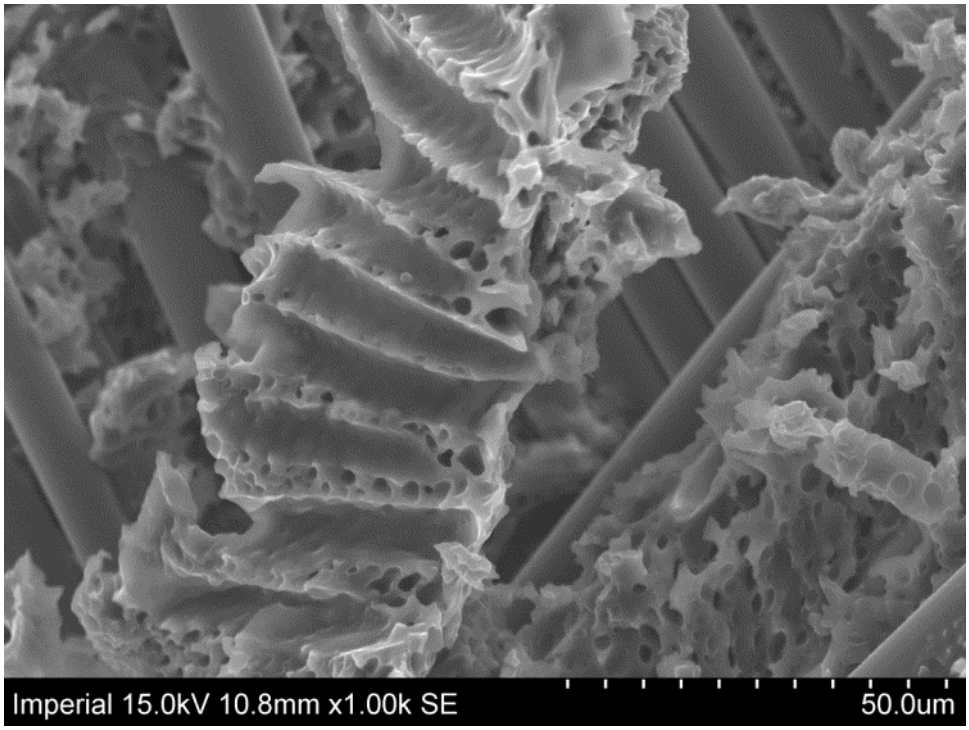

Figure 8 Sheathing of the matrix over the fibres in Device B (*Baseline Multifunctional*). N.B. Number below the scale bar indicates its full extent.

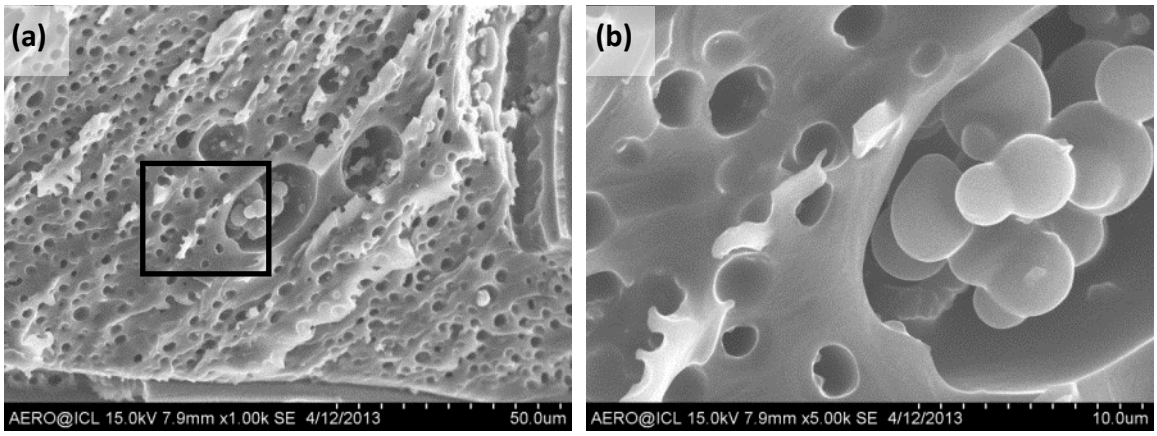

Figure 9 Pockets of structural matrix beads in Device C (*CNT Grafted Multifunctional conc1*). N.B. Number below the scale bar indicates its full extent.

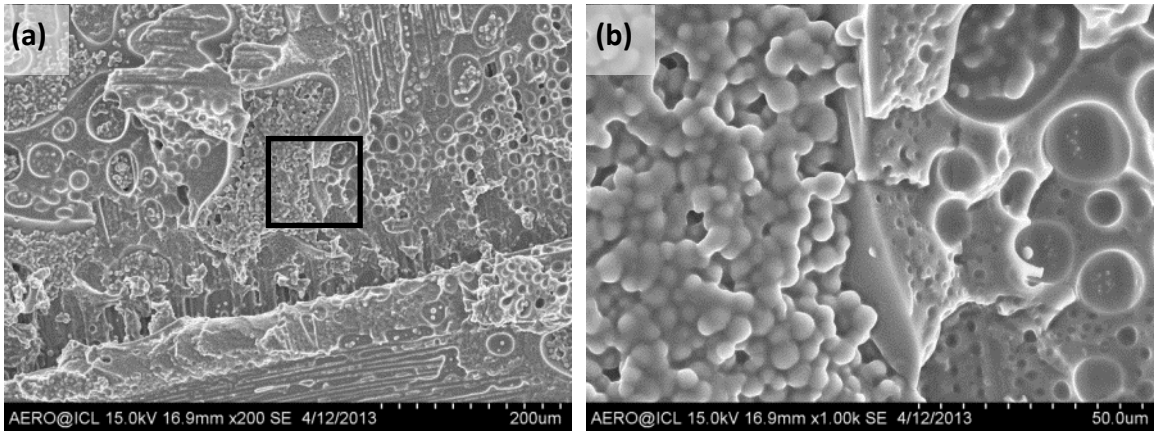

Figure 10 'Island and sea' morphology of the matrix in Device D (*CNT Grafted Multifunctional conc2*). N.B. Number below the scale bar indicates its full extent.

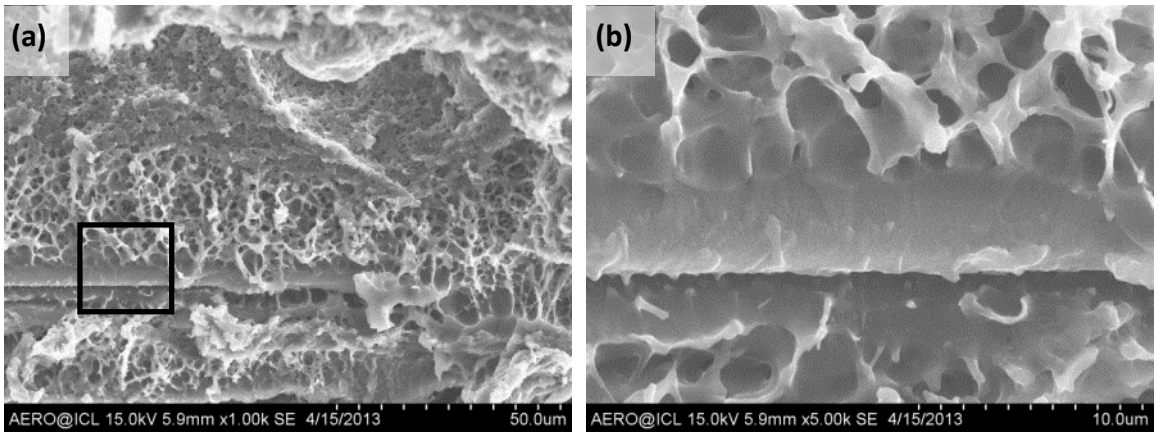

Figure 11 Localised phase distributions in Device E (*CNT Sized Multifunctional conc 1*). N.B. Number below the scale bar indicates its full extent.

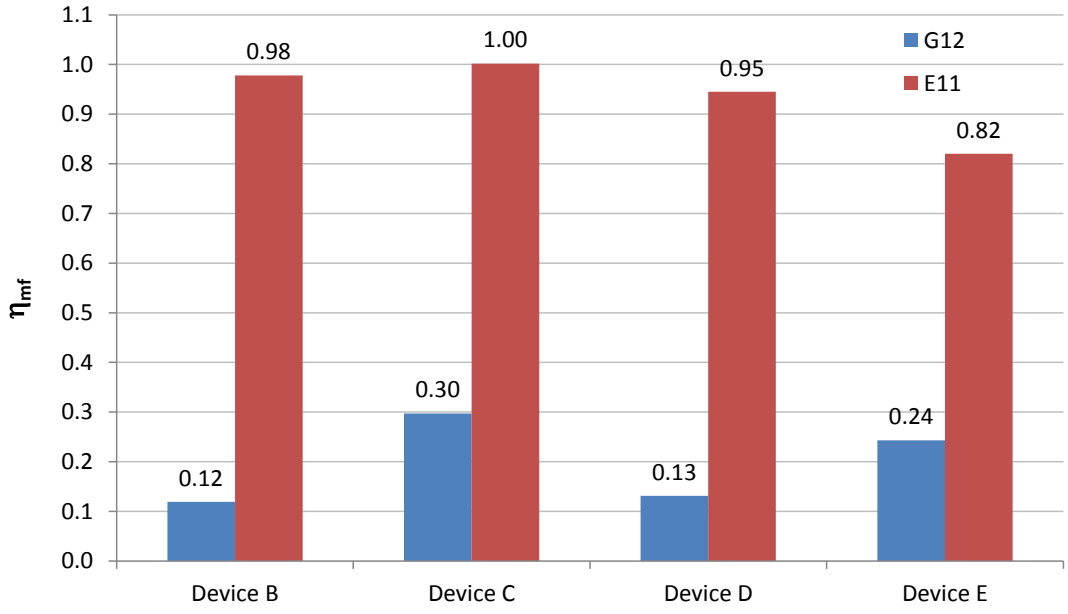

Figure 12 Multifunctional efficiencies (η_{mf}) for In-plane shear (blue) and normalised Young's (red) moduli of Device B (*Baseline multifunctional*), Device C (*CNT Grafted Multifunctional conc1*), Device D (*CNT Grafted Multifunctional conc2*) and Device E (*CNT Sized Multifunctional conc1*).